JGR Space Physics

RESEARCH ARTICLE
10.1029/2023JA032131

Key Points:

- An analytical solution for the long-standing problem of the exact Euler potentials mapping in the ionosphere is found
- The mapping is applied to the International Geomagnetic Reference Field magnetic field
- It is also applicable for other models, including T04

Correspondence to:

E. Romashets,
eromashets@lamar.edu

Citation:

Romashets, E., & Vandas, M. (2024). Exact alpha-beta mapping of IGRF magnetic field in the ionosphere. *Journal of Geophysical Research: Space Physics*, *129*, e2023JA032131. https://doi.org/10.1029/2023JA032131

Received 28 SEP 2023
Accepted 18 DEC 2023

Author Contributions:

Conceptualization: E. Romashets, M. Vandas
Data curation: E. Romashets, M. Vandas
Formal analysis: E. Romashets, M. Vandas
Funding acquisition: E. Romashets, M. Vandas
Investigation: E. Romashets, M. Vandas
Methodology: E. Romashets, M. Vandas
Project Administration: E. Romashets, M. Vandas
Resources: E. Romashets, M. Vandas
Software: E. Romashets, M. Vandas
Supervision: E. Romashets, M. Vandas
Validation: E. Romashets, M. Vandas
Visualization: E. Romashets, M. Vandas
Writing – original draft: E. Romashets, M. Vandas
Writing – review & editing: E. Romashets, M. Vandas

Exact Alpha-Beta Mapping of IGRF Magnetic Field in the Ionosphere

E. Romashets[1] and M. Vandas[2]

[1]Department of Physics, Lamar University, Beaumont, TX, USA, [2]Astronomical Institute of the Czech Academy of Sciences, Prague, Czech Republic

Abstract Finding the magnetic flux mapping in the ionosphere is very important. It would not only divide the surface into the elements with the same flux, but also indicate locations of conjugated points. It is important for studies of field aligned currents and bouncing of energetic charged particles and their precipitation. The existing methods involve numerical magnetic field lines tracing in the entire volume of the magnetosphere or numerical integration along assumed contour lines of the Euler potentials on the surface of the ionosphere. It is possible to determine the mapping with these methods near the magnetic equator, but not on middle latitudes and near and inside the polar caps. Our approach is to search for the Euler potentials as a sum of basic functions with their coefficients. Each basic function is a product of a sine or cosine of longitude multiplied by m and the Legendre polynomial of the colatitude angle cosine and of the order n. Maxima of m and n in this calculation were set to 13. The difference between the radial component from the cross product of the Euler potentials gradients and from International Geomagnetic Reference Field is less than 0.01 percent. We discuss the possibility of using orthogonal coordinates defined on the sphere's surface, which remain finite functions of θ and φ everywhere except for the vicinities of the North and South poles. The issues with numerical errors accumulated on long tracing are avoided when using this approach.

Plain Language Summary Finding the magnetic flux mapping in the ionosphere is very important. It would not only divide the surface into the elements with the number of the magnetic field lines, but also will enable us to see the exit and entry points of the same field line. It is important for studies of field aligned currents and bouncing of energetic charged particles and their precipitation in spectacular Polar Lights events. The existing methods involve long lasting integrations along model magnetic field lines in the entire volume occupied by the magnetic field. These methods cannot find the location of entry-exit points of the field lines reliably because of numerical errors accumulated on these very long calculations. Our approach is to search for the Euler potentials as a sum of basic functions with their coefficients.

1. Introduction

The Euler potentials are utilized in recent years for studying waves and related properties of solar atmosphere. Terradas and Neukirch (2023) proposed a magnetostatic model of active region using Euler potentials. Osano (2018) showed that Euler potentials may play an important role in studying the evolution of magnetic fields, in application to solar dynamo. Sweet (1950), Sakurai (1979), and Figura and Macek (2013) found that Euler potentials can describe the magnetic motion of magnetic field lines during reconnection processes. Brandenburg (2010) noticed that in numerical magnetohydrodynamic simulations with Euler potentials, presence of an artificial diffusion term leads to decaying solution, while the same simulation with a vector potential permits dynamo action. Kotarba et al. (2009) observed that the magnetic helicity vanishes in the Euler potentials representation in their modeling. Rosswog and Price (2007) assumed that the Euler potentials evolution with time should be determined by the magnetic diffusivity. Dolag and Stasyszyn (2009) performed several tests and concluded that Euler potentials can be superior for the magnetic field because of the difficulty in preserving the solenoidality condition. Webb et al. (2010) studied Alfven waves with Euler potentials and depicted the field lines in the waves.

Stern (1967) developed a technique for numerical determination of the Euler potentials contour lines on the spherical surface. The approach was the utilization of the equity

$$B_r\, l_\alpha\, l_\beta\, \sin\gamma = \Delta\alpha\ \Delta\beta, \tag{1}$$

along the isolines of α and β. Magnetic flux through a given element of the mesh equals to the product of α and β increments. Here, B_r is the radial component of the magnetic field, while l_α and l_β are the sides of the parallelogram shaped mesh element on the surface corresponding to the contourlines α, $\alpha + \Delta\alpha$, β, and $\beta + \Delta\beta$. The contourlines are not necessarily orthogonal and make an angle γ. One of the Euler potentials should have an extremum, minimum or maximum, on the line $B_r = 0$, a magnetic equator. In 2D and 2.5D (when all three components of the magnetic field are present but they depend only on two coordinates) problems, the Euler potentials can be found easily. The ultimate task is to determine the magnetic field lines in the volume, as well as electric current streamlines and charged particle trajectories. For example, in a cylindrical symmetry, a linear force-free magnetic field has the same filed lines as the current streamlines. But the cylindrically symmetric non-linear force-free magnetic field will have different magnetic field lines and current streamlines. In 3D problems, the finding of Euler potentials seems to be an impossible task. Two scalar functions, each depending on all three coordinates are to be found. This is why many instead of solving the problem of finding the Euler potentials for a given magnetic field configuration, one assumes that the Euler potentials are of pre-determined form, and then the magnetic field is

$$\mathbf{B} = \nabla\alpha \times \nabla\beta. \tag{2}$$

In fact, the problem of finding of Euler potentials for a given magnetic field can be solved. The fact that the Euler potentials are not unique is a key here. The first potential, α, could be chosen as any smooth function of B_r in the volume, provided that at any sphere it reaches a minimum or maximum on the line where the radial component of the magnetic field is zero. Second Euler potential then can be found by various methods, for example, the least squares one, by selection of the coefficients near the basic functions in the volume. Another numerical method of $\alpha - \beta$ determination was developed by Peymirat and Fontaine (1999), and used for the T87 Tsyganenko model (Tsyganenko, 1987). It requires field line tracing through the entire magnetosphere, which can accumulate numerical errors. Zaharia (2008) used pre-determined Euler potentials for setting flux coordinates in numerical iterative procedure for studies of Tsyganenko T96 model magnetosphere (Tsyganenko & Stern, 1996). Dungey (1963) proposed a simple model of α for combined dipole and induced by the magnetopause currents magnetic fields, while β was the same as for a dipole, $\beta = \varphi$, the longitudinal angle in dipole reference system. Schulz and Chen (2008) introduced a generalization into the model by assuming the Dungey parameter b to be a function of the longitudinal angle. This enabled an analysis of the ring current and phenomena associated with it. Goertz (1976) used his analytical α and β for combined magnetic dipole field and one induced by equatorial current sheet on Jupiter. Khurana (1997) adopted the Goertz (1976) approach and proposed a modification taking into account the complicated realistic shape of Jupiter's current sheet and the current distribution on it.

The Euler potentials for two parallel and antiparallel current-carrying wires in the homogeneous ambient magnetic field were found in Romashets and Vandas (2011). The magnetic field and Euler potentials of two parallel and antiparallel current sheets in homogeneous ambient magnetic field, with uniform and non-uniform distribution of currents on sheets of zero thickness were studied in Romashets and Vandas (2012) and Vandas and Romashets (2016). The current sheets of finite thickness in the ambient magnetic field, and combined magnetic field with the Euler potentials were determined in Vandas and Romashets (2014). The Euler potentials for the Earth's dipole magnetic field, field-aligned currents, and the ring current were found in Romashets and Vandas (2020). The Dungey (Dungey, 1963) term was added into the consideration in Romashets and Vandas (2022).

2. Method

We look for the Euler potentials on the sphere of radius a, the two scalar functions of colatitude and longitude, $\alpha(\theta, \varphi)$ and $\beta(\theta, \varphi)$. The Equation 1 used in Stern (1967) with infinitesimally small steps along the α and β directions is equivalent to the Equation 2, which simplifies now to:

$$B_r = \frac{1}{a^2 \sin\theta}\left(\frac{\partial\alpha}{\partial\theta}\frac{\partial\beta}{\partial\varphi} - \frac{\partial\alpha}{\partial\varphi}\frac{\partial\beta}{\partial\theta}\right). \tag{3}$$

Here,

$$B_r = -\frac{\partial V}{\partial r} \tag{4}$$

is the radial component of the International Geomagnetic Reference Field (IGRF) (Alken et al., 2021), the link is https://www.ncei.noaa.gov/products/international-geomagnetic-reference-field, with a scalar potential

$$V = a\sum_{n=1}^{13}\sum_{m=0}^{n}\left(\frac{a}{r}\right)^{n+1}P_n^m(\cos\theta)(g_{nm}\cos m\varphi + h_{nm}\sin m\varphi). \quad (5)$$

Here, P_n^m are Schmidt normalized associated Legendre functions. The IGRF coefficients are h_{nm} and g_{nm}, while $a = 6371.2$ km is the Earth's radius. The angles θ and φ are in the geocentric coordinate system (Russell, 1971). The first Euler potential is chosen as

$$\alpha = a^2\sqrt{4.5B_0^2 - B_r^2}. \quad (6)$$

Here, $B_0 = 35{,}000$ nT is the average magnetic field magnitude on the Earth's surface. The contour lines of this potential are shown in top panel of Figure 1. It reaches its maximum on the magnetic equator line, where $B_r = 0$. The second Euler potential is searched as a sum of basic functions on the spherical surface,

$$\beta = \sum_{n=0}^{N}\sum_{m=0}^{M}c_{nm}P_n(\cos\theta)\cos m\varphi + \sum_{n=0}^{N}\sum_{m=1}^{M}d_{nm}P_n(\cos\theta)\sin m\varphi = \sum_{i=1}^{I}e_i\beta_i. \quad (7)$$

This Euler potential is in units of the magnetic flux, nT km^2. The term for $n = 0$, m = 0, c_{00} is replaced by $c_{00}\,\varphi$, to avoid a constant with zero gradient. The coefficients e_i in Equation 7 are determined by using the least squares method, with the matrix elements

$$M_{ij} = \int_0^{\pi}\int_0^{2\pi}\left(\frac{\partial\alpha}{\partial\theta}\frac{\partial\beta_i}{\partial\varphi} - \frac{\partial\alpha}{\partial\varphi}\frac{\partial\beta_i}{\partial\theta}\right)\left(\frac{\partial\alpha}{\partial\theta}\frac{\partial\beta_j}{\partial\varphi} - \frac{\partial\alpha}{\partial\varphi}\frac{\partial\beta_j}{\partial\theta}\right)\frac{\mathrm{d}\theta\,\mathrm{d}\varphi}{a^2\sin\theta}. \quad (8)$$

The right hand side vector's elements are

$$R_i = -\int_0^{\pi}\int_0^{2\pi}\left(\frac{\partial\alpha}{\partial\theta}\frac{\partial\beta_i}{\partial\varphi} - \frac{\partial\alpha}{\partial\varphi}\frac{\partial\beta_i}{\partial\theta}\right)\mathrm{d}\theta\,\mathrm{d}\varphi. \quad (9)$$

3. Results

The solution of the least squares method linear system of equations was obtained and used for the calculation of the radial component of the magnetic field. The radial component calculated from α and β and one from IGRF are practically the same. The contour lines of the calculated β are shown in bottom panel of Figure 1. Very close to the $B_r = 0$ line, the contour lines of α and β are almost parallel, that is their gradients aligned, which leads to very small cross product of the two gradients, which provides a small calculated radial component. Further away from the magnetic equator, the gradients are not aligned. The IGRF B_r component is shown in top panel of Figure 2, while one calculated with the model α and β is depicted in middle panel of Figure 2. The difference is very small, as one can see in bottom panel of Figure 2, where the percentage difference between IGRF and Euler potential representation is given.

4. Conclusions and Discussion

The exact Euler potential mapping method is presented and used for the ionosphere with IGRF magnetic field. The location of conjugated points can be determined with any prescribed accuracy. The results can be used for modeling of field–aligned currents and shell currents in the ionosphere. The basic functions in Equation 7 enable us to fit the radial component with mapped α and β very well. The assumptions on the specific nature of the Euler potentials which were used: one of the Euler potentials should have an extremum on the line $B_r = 0$. No other assumptions are needed. The second Euler potential is found by selection of the coefficients near the basic functions. The meaning of the basic functions is that they form a basis, that is any function of θ and φ on the sphere can be constructed with these functions. The alternative here is to use specific arguments and build the Euler potentials with them, as described below. It was shown in Romashets and Vandas (2011) that the Euler potentials

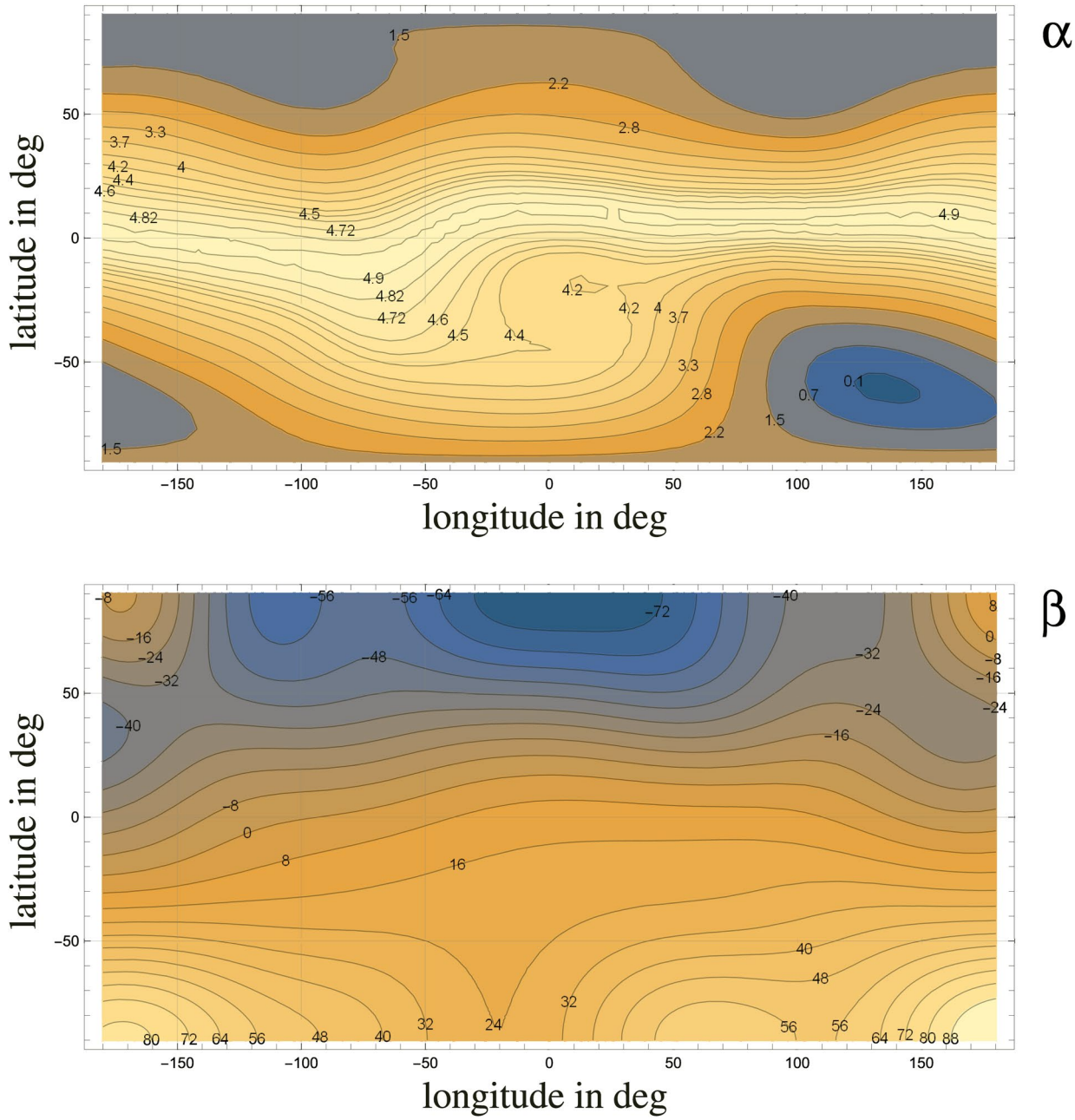

Figure 1. Contourlines of the Euler potentials (top panel) α and (bottom panel) β as functions of longitude φ and latitude $\lambda = \theta - \frac{\pi}{2}$.

α and β expressed in terms of orthogonal magnetic coordinates μ and η can be very useful for describing various magnetic fields. We use this idea for IGRF mapping in the ionosphere. On the sphere $r = a$, two scalar functions $\alpha(\theta, \varphi)$ and $\beta(\theta, \varphi)$, which satisfy

$$B_r \hat{\mathbf{e}}_\mathbf{r} = \nabla\alpha \times \nabla\beta \tag{10}$$

are to be found. The Equation 10 is equivalent to the condition that the flux through a single element of the mesh is a product of increments along α and β

$$|\Delta\alpha\, \Delta\beta| = |B_r\, \mathbf{l}_\alpha \times \mathbf{l}_\beta|, \tag{11}$$

which is used in numerical identifications of $\alpha = \text{const}$ and $\beta = \text{const}$ isolines. The mesh element is a parallelogram with the sides l_α and l_β. It is convenient to deal with two orthogonal functions of the same magnitude of

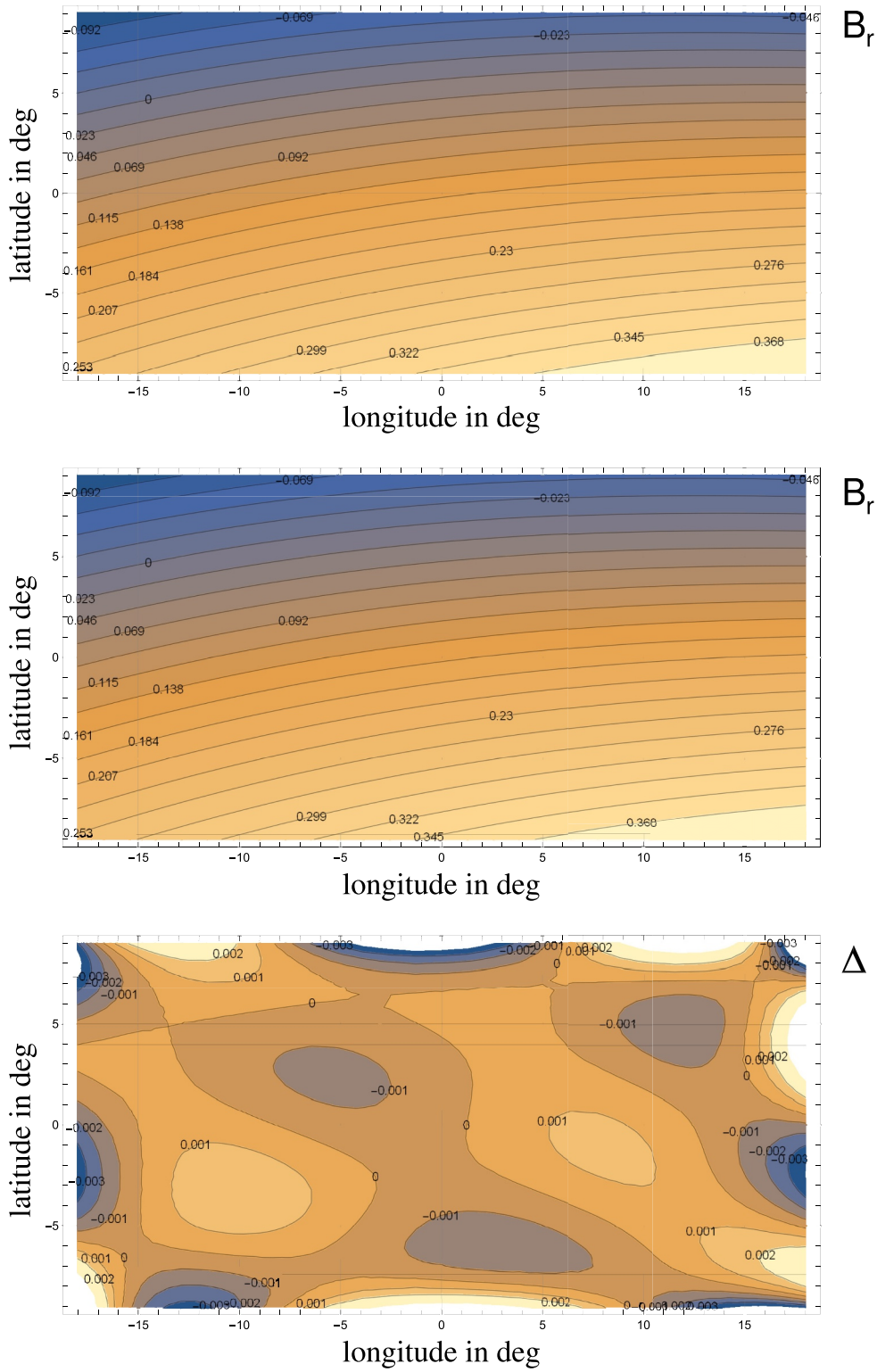

Figure 2. International Geomagnetic Reference Field (IGRF) radial component B_r near the center of the map (top panel), the calculated with α and β radial component B_r (middle panel), and the percentage difference between the model and IGRF B_r (bottom panel) as functions of longitude φ and latitude $\lambda = \theta - \frac{\pi}{2}$.

the gradient. We are looking for two sums of correspondingly orthogonal functions, and the gradients of two functions perpendicular to each other and equal in magnitude. In other words,

$$\alpha = \sum_{i=1}^{N} c_i [f(\theta, \varphi)]^i, \quad \beta = \sum_{i=1}^{N} d_i [g(\theta, \varphi)]^i \tag{12}$$

with

$$|\nabla f \times \nabla g| = (\nabla f)^2. \tag{13}$$

Each function in the sums is

$$f = u(\theta) v(\varphi), \quad g = t(\theta) s(\varphi). \tag{14}$$

The pair of conditions from Romashets and Vandas (2011) reads

$$\frac{\partial f}{\partial \theta} = \frac{1}{\sin\theta} \frac{\partial g}{\partial \varphi}, \quad \frac{1}{\sin\theta} \frac{\partial f}{\partial \varphi} = -\frac{\partial g}{\partial \theta}. \tag{15}$$

It is equivalent to

$$u' v \sin\theta = t s', \quad u v' = -t' s \sin\theta. \tag{16}$$

For the functions of θ, we have

$$\frac{u' \sin\theta}{t} = k_1, \quad \frac{u}{t' \sin\theta} = -k_2. \tag{17}$$

Here, k_1 and k_2 are constants to apply separation of variables method. Isolating u from the second equation in Equation 17 and taking its derivative, we can substitute it into the first equation and obtain an equation for t:

$$k_1 t + k_2 t' \cos\theta \sin\theta + k_2 t'' \sin^2\theta = 0. \tag{18}$$

We can look for t as a function of $\cos\theta$, and Equation 18 becomes

$$k_1 t - 2k_2 t' \cos\theta \sin^2\theta + k_2 t'' \sin^4\theta = 0. \tag{19}$$

The solutions are

$$t = \cos\left(\frac{1}{2}\sqrt{\frac{k_1}{k_2}} \ln\frac{1-\cos\theta}{1+\cos\theta} - \phi_1\right), \; u = \sin\left(\frac{1}{2}\sqrt{\frac{k_1}{k_2}} \ln\frac{1-\cos\theta}{1+\cos\theta} - \phi_1\right). \tag{20}$$

For the functions of φ, one can get similar to Equation 17 system:

$$\frac{s'}{v} = k_1, \quad -\frac{s}{v'} = -k_2. \tag{21}$$

Omitting the details, the v and s are

$$v = \cosh\sqrt{\frac{k_1}{k_2}}(\varphi - \varphi_2), \quad s = \sinh\sqrt{\frac{k_1}{k_2}}(\varphi - \varphi_2). \tag{22}$$

We can introduce a new constant $k = \frac{1}{i}\sqrt{\frac{k_1}{k_2}}$. Here, i is an imaginary unit. Then the general form of f and g is

$$f = \cosh\left(\frac{k}{2} \ln\frac{1-\cos\theta}{1+\cos\theta} - \phi_1\right) \cos\, k(\varphi - \phi_2) \tag{23}$$

and

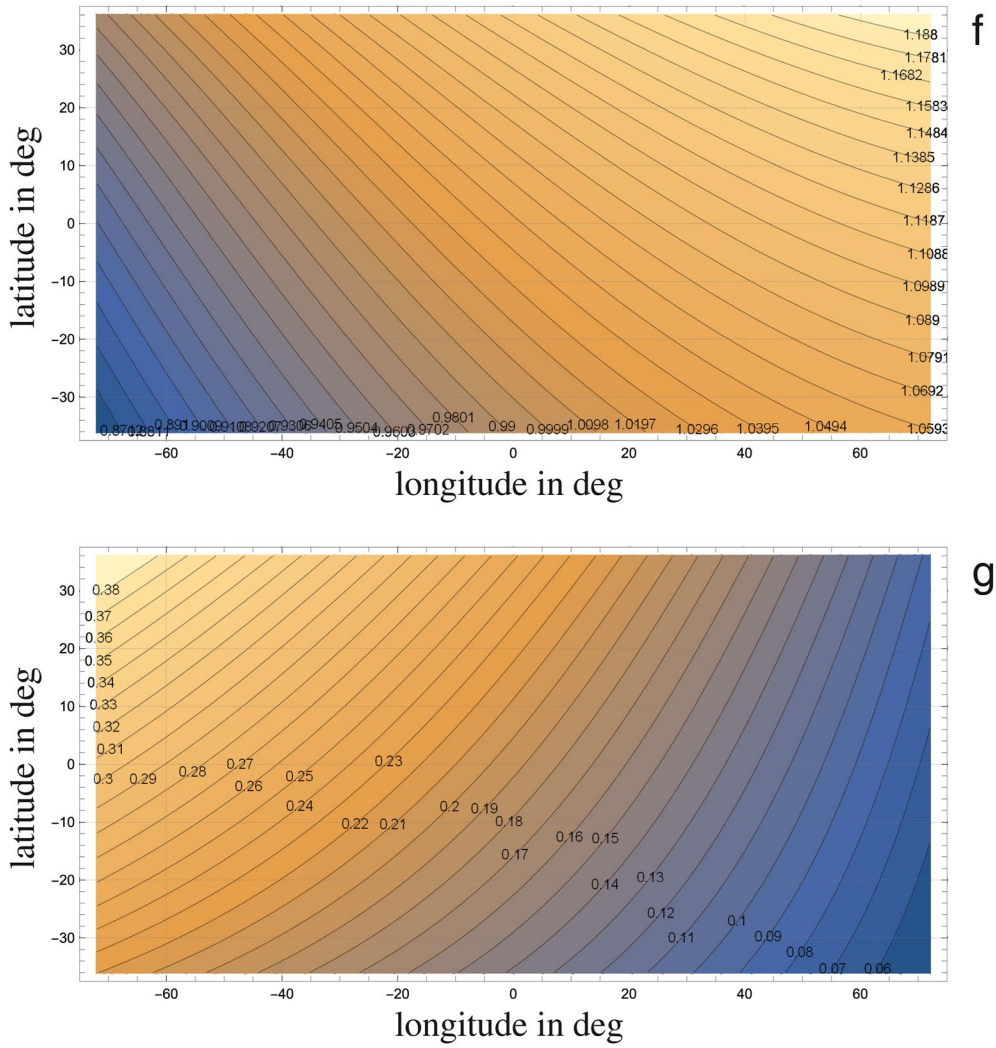

Figure 3. Typical contours of coordinates f in Equation 23 (top panel) and g in Equation 24 (bottom panel) as functions of longitude φ and latitude $\lambda = \theta - \frac{\pi}{2}$.

$$g = \sinh\left(\frac{k}{2}\ln\frac{1-\cos\theta}{1+\cos\theta} - \phi_1\right)\sin k\,(\varphi - \phi_2). \tag{24}$$

The typical contourlines of the orthogonal coordinates Equations 23 and 24 are shown in Figure 3, with $k = 0.2$, $\phi_1 = 0.5$, and $\phi_2 = 1.9$. In this alternative approach, one Euler potential is constructed from the condition mentioned above, and the second potential should then actually satisfy Equation 10. The alternative approach described here has an advantage that the variables are orthogonal and together with $\mathbf{r}$ can form a system of coordinates. On the other hand, Equations 23 and 24 are not finite at the poles, $\theta = 0$ and $\theta = \pi$, while the basic functions in Equation 7 are. This former observation can be reformulated that the alternative pair of Euler potentials can be determined with the coordinates f and g very precisely on any region of the sphere except for the vicinities of the poles. In order to compute α, we choose the non-linear parameters in a way that the linear coefficients c_1, c_2, and c_3 can be then easily selected for the left part of Equation 12 to be very close to $B_r^2 a^2 / B_0$. That means, N is 3, and the minimum variance simplifies to three equations

$$\begin{aligned}
\int_{\theta_1}^{\theta_2}\int_{\varphi_1}^{\varphi_2}\left(c_1 f^2 + c_2 f^3 + c_3 f^4\right)\sin\theta\,\mathrm{d}\theta\,\mathrm{d}\varphi &= \int_{\theta_1}^{\theta_2}\int_{\varphi_1}^{\varphi_2} f\,\frac{B_r^2}{B_0^2}\sin\theta\,\mathrm{d}\theta\,\mathrm{d}\varphi,\\
\int_{\theta_1}^{\theta_2}\int_{\varphi_1}^{\varphi_2}\left(c_1 f^3 + c_2 f^4 + c_3 f^5\right)\sin\theta\,\mathrm{d}\theta\,\mathrm{d}\varphi &= \int_{\theta_1}^{\theta_2}\int_{\varphi_1}^{\varphi_2} f^2\,\frac{B_r^2}{B_0^2}\sin\theta\,\mathrm{d}\theta\,\mathrm{d}\varphi,\\
\int_{\theta_1}^{\theta_2}\int_{\varphi_1}^{\varphi_2}\left(c_1 f^4 + c_2 f^5 + c_3 f^6\right)\sin\theta\,\mathrm{d}\theta\,\mathrm{d}\varphi &= \int_{\theta_1}^{\theta_2}\int_{\varphi_1}^{\varphi_2} f^3\,\frac{B_r^2}{B_0^2}\sin\theta\,\mathrm{d}\theta\,\mathrm{d}\varphi.
\end{aligned} \tag{25}$$

If the solution of Equation 25,

$$\alpha = c_1 f + c_2 f^2 + c_3 f^3, \tag{26}$$

does not fit $B_r a^2/B_0$ well, then the non-linear free parameters k, ϕ_1, and ϕ_2 are adjusted, with non-linear methods. Once the fit is good, then N is increased, so the match is exact. The second Euler potential, β, is constructed first with only three terms, for which the minimum variance linear system is

$$\begin{aligned}
\int_{\theta_1}^{\theta_2}\int_{\varphi_1}^{\varphi_2}\left(d_1 + 2d_2 g + 3d_3 g^2\right)(\nabla f)^4\left(\frac{\partial\alpha}{\partial f}\right)^2\sin\theta\,\mathrm{d}\theta\,\mathrm{d}\varphi &= \pm\int_{\theta_1}^{\theta_2}\int_{\varphi_1}^{\varphi_2} B_r\,\frac{\partial\alpha}{\partial f}(\nabla f)^2\sin\theta\,\mathrm{d}\theta\,\mathrm{d}\varphi,\\
\int_{\theta_1}^{\theta_2}\int_{\varphi_1}^{\varphi_2}\left(2gd_1 + 4d_2 g^2 + 6d_3 g^3\right)(\nabla f)^4\left(\frac{\partial\alpha}{\partial f}\right)^2\sin\theta\,\mathrm{d}\theta\,\mathrm{d}\varphi &= \pm\int_{\theta_1}^{\theta_2}\int_{\varphi_1}^{\varphi_2} 2g\,B_r\,\frac{\partial\alpha}{\partial f}(\nabla f)^2\sin\theta\,\mathrm{d}\theta\,\mathrm{d}\varphi,\\
\int_{\theta_1}^{\theta_2}\int_{\varphi_1}^{\varphi_2}\left(3g^2 d_1 + 6d_2 g^3 + 9d_3 g^4\right)(\nabla f)^4\left(\frac{\partial\alpha}{\partial f}\right)^2\sin\theta\,\mathrm{d}\theta\,\mathrm{d}\varphi &= \pm\int_{\theta_1}^{\theta_2}\int_{\varphi_1}^{\varphi_2} 3g^2\,B_r\,\frac{\partial\alpha}{\partial f}(\nabla f)^2\sin\theta\,\mathrm{d}\theta\,\mathrm{d}\varphi.
\end{aligned}$$

The free parameters cannot be adjusted at this step. If the agreement between the original radial component of the magnetic field and that calculated with the Euler potentials is not good, then more coefficients are added, in order to reach the match. The meaning of $\pm$ in the equations above is that two sets of the coefficients d_1, d_2, and d_3 are found separately for the region where B_r is positive and where it is negative. When determining the positive region, the integrand on both sides of the equation is zero when $B_r < 0$ and vice versa. The β potential on the positive region contains the coefficients from that region, and the positive one—from the positive region. The good agreement between the calculated and actual B_r is the criterion for choosing the method with which the Euler coefficients will be found. One with orthogonal contourlines seems to be more natural but it is more complicated. The $\alpha - \beta$ mapping enables locating of entry and exit points of the magnetic field lines into and out of the ionosphere but not the line itself between the two points. The problem of finding the magnetic field lines in the magnetosphere will be solved in the future, by applying a similar approach. The first Euler potential, α, is a function of B_r^2, and β will be determined from the integrations of the basic functions in the volume and solving corresponding matrix equation. For spherically symmetric model magnetospheric magnetic field, when β can be chosen as $\beta = -\varphi$, this problem was solved in Romashets and Vandas (2022).

The purpose of this study was to find an alpha-beta mapping of the IGRF. It was noticed that the method is applicable to any magnetic field, one induced by the currents inside the sphere, outside of it, and on it. The changes of the mapping caused for example, by increased ring current can be observed. This will be done in a separate future work.

Data Availability Statement

Data on IGRF coefficients is available through Alken et al. (2021).

Acknowledgments
The authors wish to express sincere thanks to many colleagues for fruitful discussions and deep insight into the problems to be solved. Especially useful comments were made by Stefaan Poedts. This work was supported by the NSF Grant 2230363. M. V. acknowledges support from the AV ČR Grant RVO:67985815 and the GAČR Grant 21-26463S.

References

Alken, P., Thébault, E., Beggan, C. D., Amit, H., Aubert, J., Baerenzung, J., et al. (2021). International geomagnetic reference field: The thirteenth generation. *Earth Planets and Space*, *73*(1), 25. ID49. https://doi.org/10.1186/s40623-020-01288-x

Brandenburg, A. (2010). Magnetic field evolution in simulations with Euler potentials. *Monthly Notices of the Royal Astronomical Society*, *401*(1), 347–354. https://doi.org/10.1111/j.1365-2966.2009.15640.x

Dolag, K., & Stasyszyn, F. A. (2009). An MHD GADGET for cosmological simulations. *Monthly Notices of the Royal Astronomical Society*, *398*(4), 1678–1697. https://doi.org/10.1111/j.1365-2966.2009.15181.x

Dungey, J. W. (1963). The structure of the exosphere or adventures in velocity space. In C. DeWitt, J. Hieblot, & A. Lebeau (Eds.), *Geophysics, the Earth's environment* (pp. 503–550). Gordon and Breach.

Figura, P., & Macek, W. (2018). Model of line preserving field line motions using Euler potentials. *Annals of Physics*, *333*, 127–135. https://doi.org/10.1016/j.aop.2013.03.004

Goertz, C. K. (1976). The current sheet in Jupiter's magnetosphere. *Journal of Geophysical Research*, *81*(19), 3368–3372. https://doi.org/10.1029/ja081i019p03368

Khurana, K. K. (1997). Euler potential models of Jupiter's magnetospheric field. *Journal of Geophysical Research*, *102*(A6), 11295–11306. https://doi.org/10.1029/97ja00563

Kotarba, H., Lesch, H., Dolag, K., Naab, T., Johansson, P. H., & Stasyszyn, F. A. (2009). Magnetic field structure due to the global velocity field in spiral galaxies. *Monthly Notices of the Royal Astronomical Society*, *397*(2), 733–747. https://doi.org/10.1111/j.1365-2966.2009.15030.x

Osano, B. (2018). Dynamo theory, nonlinear magnetic fields, and the Euler potentials. *Advances in Astronomy*, *2018*, 6. ID4823494. https://doi.org/10.1155/2018/4823494

Peymirat, C., & Fontaine, D. (1999). A numerical method to compute Euler potentials for non dipolar magnetic fields. *Annales Geophysicae*, *17*(3), 328–337. https://doi.org/10.1007/s005850050762

Romashets, E. P., & Vandas, M. (2011). Euler potentials for two line currents aligned with an ambient uniform magnetic field. *Journal of Geophysical Research*, *116*(A9), 9. IDA09227. https://doi.org/10.1029/2011ja016595

Romashets, E. P., & Vandas, M. (2012). Euler potentials for two current sheets along ambient uniform magnetic field. *Journal of Geophysical Research*, *117*(A7), 8. IDA07221. https://doi.org/10.1029/2012ja017587

Romashets, E. P., & Vandas, M. (2020). Euler potentials for the Earth magnetic field with field-aligned currents. *Journal of Geophysical Research: Space Physics*, *125*(8), 11. IDe28153. https://doi.org/10.1029/2020ja028153

Romashets, E. P., & Vandas, M. (2022). Euler potentials for Dungey magnetosphere with axisymmetric ring and field-aligned currents. *Journal of Geophysical Research: Space Physics*, *127*(3), 13. IDe30171. https://doi.org/10.1029/2021ja030171

Rosswog, S., & Price, D. J. (2007). MAGMA: A three-dimensional, Lagrangian magnetohydrodynamics code for merger applications. *Monthly Notices of the Royal Astronomical Society*, *379*(3), 915–931. https://doi.org/10.1111/j.1365-2966.2007.11984.x

Russell, C. T. (1971). Geophysical coordinate transformations. *Cosmic Electrodynamics*, *2*, 184–196.

Sakurai, T. (1979). A new approach to the force-free field and its application to the magnetic field of solar active regions. *Publications of the Astronomical Society of Japan*, *31*, 209–230.

Schulz, M., & Chen, M. (2008). Field-line (Euler-potential) model of the ring current. *Journal of Atmospheric and Solar-Terrestrial Physics*, *70*(2–4), 482–489. https://doi.org/10.1016/j.jastp.2007.08.063

Stern, D. (1967). Geomagnetic Euler potentials. *Journal of Geophysical Research*, *72*(15), 3995–4005. https://doi.org/10.1029/jz072i015p03995

Sweet, P. A. (1950). The effect of turbulence on a magnetic field. *Monthly Notices of the Royal Astronomical Society*, *110*(1), 69–83. https://doi.org/10.1093/mnras/110.1.69

Terradas, J., & Neukirch, T. (2023). Three-dimensional solar active region magnetohydrostatic models and their stability using Euler potentials. *Astronomy and Astrophysics*, *671*, 15. A31. https://doi.org/10.1051/0004-6361/202244687

Tsyganenko, N. A. (1987). Global quantitative models of the geomagnetic field in the cislunar magnetosphere for different disturbance levels. *Planetary and Space Science*, *35*(11), 1347–1358. https://doi.org/10.1016/0032-0633(87)90046-8

Tsyganenko, N. A., & Stern, D. P. (1996). Modeling the global magnetic field of the large-scale Birkeland current system. *Journal of Geophysical Research*, *101*(A12), 27187–27198. https://doi.org/10.1029/96ja02735

Vandas, M., & Romashets, E. P. (2014). Euler potentials for two current sheets of nonzero thickness along ambient uniform magnetic field. *Journal of Geophysical Research: Space Physics*, *119*(4), 2579–2592. https://doi.org/10.1002/2013ja019604

Vandas, M., & Romashets, E. P. (2016). Euler potentials for two layers with non-constant current densities in the ambient magnetic field aligned to the layers. *Annales Geophysicae*, *34*(12), 1165–1173. https://doi.org/10.5194/angeo-34-1165-2016

Webb, G. M., Hu, Q., Dasgupta, B., Roberts, D. A., & Zank, G. P. (2010). Alfven simple waves: Euler potentials and helicity. *The Astronomical Journal*, *725*(2), 2128–2151. https://doi.org/10.1088/0004-637x/725/2/2128

Yahalom, A., & Lynden-Bell, D. (2008). Simplified variational principles for barotropic magnetohydrodynamics. *Journal of Fluid Mechanics*, *607*, 235–265. https://doi.org/10.1017/s0022112008002024

Zaharia, S. (2008). Improved Euler potential method for three-dimensional magnetospheric equilibrium. *Journal of Geophysical Research*, *113*(A8), 7. A08221. https://doi.org/10.1029/2008ja013325